PERGAMON

Chaos, Solitons and Fractals 14 (2002) 403–423

CHAOS
SOLITONS & FRACTALS

www.elsevier.com/locate/chaos

Bifurcations and onset of chaos on the ergodic magnetic limiter mapping

Elton C. da Silva [a,*], Iberê L. Caldas [a], Ricardo L. Viana [b]

[a] *Instituto de Física, Universidade de São Paulo, CP 66318, 05315-970, São Paulo, Brazil*
[b] *Departamento de Física, Universidade Federal do Paraná, CP 19081, 81531-990, Curitiba, Paraná, Brazil*

Accepted 15 June 2001

Abstract

We propose a Hamiltonian formulation to study the magnetic field line structure in a tokamak with ergodic magnetic limiter. An analytical stroboscopic mapping, derived from this formulation, is used to investigate the onset of global field line chaos at the plasma edge and the Hamiltonian bifurcations of magnetic axes.

1. Introduction

Among the large number of fusion-oriented plasma devices, the tokamak seems to be one of the most promising candidates for a future thermonuclear power plant. Many factors conspire against the obtention of long lasting plasma confinement in tokamaks, however [1,2]. One of them is the ubiquitous presence of plasma instabilities, that may destroy plasma confinement due to a variety of causes [3–5]. Another major problem in tokamak physics is the control of plasma contamination by impurities released from the inner wall by surface processes [6].

Tokamaks are toroidal pinches in which plasmas are generated by ohmic heating of a filling gas and confined by externally applied magnetic fields: a toroidal field produced by external coils, and a poloidal field generated by the plasma column itself [1,2]. This combination will be called the equilibrium field. The corresponding magnetic field lines have helical shape so that, at least in a first approximation, particles are confined by them. We may think of these field lines as lying on magnetic surfaces with topology of nested tori.

From the point of view of a magnetohydrodynamical (MHD) theory, these surfaces are also isobaric ones, on which the plasma expansion caused by a pressure gradient is counterbalanced by the Lorentz force resulting from the interaction between the equilibrium magnetic field and the plasma electric current density. The existence of closed toroidal magnetic surfaces is a necessary, albeit not sufficient, condition for plasma confinement in tokamaks [3,7].

In order to control the abovementioned plasma–wall interactions, that may lead to loss of confinement, it has been proposed to create a cold boundary layer of chaotic field lines in the periphery of the tokamak vessel [8–10]. This region comprises the outer plasma column and the vacuum region that surrounds it from the inner tokamak wall. This can be accomplished by destroying some, but not all, magnetic surfaces located in this region. A way to do this, without spoiling the plasma column itself, is to generate external magnetic fields that interact with the equilibrium field and cause a selective destruction of magnetic surfaces, which is the basic principle of the ergodic magnetic limiter concept.

Chaotic magnetic field lines are taken here from a magneto-static perspective, i.e., there is sensibility to initial conditions in the sense that two field line points, very close from each other, evolve through a large number of revolutions around the tokamak so that the distance between the resulting field lines deviates with a positive exponential

* Corresponding author.
E-mail address: elton@if.usp.br (E.C. da Silva).

0960-0779/02/$ - see front matter
PII: S0960-0779(01)00133-3

rate [3,7]. By identifying field line equations with canonical equations, we can build a Hamiltonian theory for the magnetic field line structure in symmetrical systems [11,12]. The equilibrium field is a one degree-of-freedom, hence integrable, Hamiltonian system. In this framework we identify magnetic surfaces with KAM tori and chaos appears from the mechanism widely understood for this type of dynamical systems [13].

The application of magnetostatic perturbations due to currents external to the tokamak vessel, causes the destruction of some, but not all, magnetic surfaces [8–10]. In the Hamiltonian theory of near-integrable systems, which is applicable if the perturbing currents are not too large, we know that some surfaces are destroyed, producing island-shaped structures that resemble the orbit structure of a nonlinear pendulum [14–16]. In the plasma physics literature these structures are named magnetic islands, and they have a complicated structure near their hyperbolic (unstable) fixed points, in the sense that the invariant manifolds that stem from these points intercept each other in a rather complicated way, forming the so-called homoclinic figure. The field line dynamics on these homoclinic points is chaotic [14].

According to the KAM theorem however, there remains a large number of surviving, albeit distorted, magnetic surfaces. They act as barriers, preventing large scale field line diffusion [12]. On the other hand, the use of an ergodic magnetic limiter requires a wide region of chaotic field lines in the tokamak periphery. The transition to such a situation occurs in an abrupt way, since one requires that no undestructed magnetic surfaces should exist between neighbor magnetic islands. If this is true, the locally chaotic regions related to each islands' separatrices may coalesce and yield large scale chaotic motion [15].

As we further increase the perturbation strength, other phenomena take place. Even after a widespread chaotic region is created, the islands' centers are still stable fixed points and surrounded by an increasingly small number of KAM tori. At some another critical perturbation intensity, however, even those centers can lose stability and become unstable. Moreover, after we reach this critical parameter value, two new stable fixed points appear. This configures a bifurcation, that has important consequences, since it implies both in the disappearance of a magnetic axis (degenerate surface with zero radius) as well as in the formation of two new magnetic axes, altering in a dramatic way the topology of magnetic confinement.

Besides the ergodic limiter, the ergodic divertor has received great attention in modern tokamak research. In the ergodic divertor, the separatrix between the last confining magnetic surface and the open surfaces is replaced by a layer of chaotic field lines that divert plasma particles to divertor plates, where they can be recycled and pumped to reduce impurity levels in the plasma [17,18]. Ergodic divertors have received treatments based on simple analytical maps for field lines [19] and more recently there were used canonical mappings from a Hamiltonian treatment [20,21]. It turns out that some simple twist maps like the Chirikov–Taylor standard map may not be appropriate to model field line behavior [22,23].

The ergodic limiter has been studied by means of a simplified mapping [15] that has been later improved with toroidal corrections and parameters describing the equilibrium and perturbed magnetic fields [24,25]. The ergodic limiter is a symmetry breaking form of perturbation, in the sense that it spoils axisymmetry of the equilibrium tokamak field. The influence of the type of symmetry-breaking perturbation was studied from the point of view of analytical and numerical field line maps [26]. A Hamiltonian treatment of ergodic limiters has been proposed in a rectangular geometry [27]. We have recently proposed a Hamiltonian map in a realistic toroidal geometry and using magnetic fields consistent with a general MHD equilibrium theory [28]. This map may be derived from the canonical equations with a field line Hamiltonian where the ergodic limiter action is supposed to be a sequence of delta-functions in the toroidal direction.

The purpose of this paper is twofold: we will study the onset of magnetic field line chaos produced by an ergodic limiter, by analyzing the interaction between adjacent magnetic islands. Secondly, we investigate bifurcations that occur before the mainly chaotic region is generated in the tokamak periphery. We will use an analytically obtained field line mapping [28]. The advantage of this procedure, in comparison with a direct numerical integration of field line equations, is the higher computation speed of map iterations compared with usual integration schemes, like predictor–corrector methods for differential equation. This difference may be crucial if long-term behavior of field lines is being considered, as in numerical studies of anomalous diffusion [29]. However, the use of oversimplified physical models for both the equilibrium and the ergodic limiter magnetic field may lead to misleading results, so that we use in this work an appropriate geometry to fully incorporate toroidicity effects, and a MHD equilibrium model from which the equilibrium field is obtained.

This paper is organized as follows: in Section 2 we present the model fields for the equilibrium and the ergodic limiter perturbation, an analytically obtained field line mapping, and an explicit form of a field line Hamiltonian. Section 3 is devoted to an application of standard perturbation techniques to describe the magnetic island structure, which gives the location and width of each island of interest. Section 4 focuses on the onset of chaos, describing the application of a modified Chirikov criterion, and discusses the conditions under which we get chaotic behavior in the tokamak

periphery. In Section 5 we study bifurcations that occur after global field line chaos. Our conclusions are left to the last section.

2. Model fields

In Fig. 1 we depict the basic tokamak geometry to be used throughout this paper. The tokamak vessel has a minor radius b and a major radius R_0, so that an aspect ratio $A = R_0/b$ can be defined. Polar coordinates (r, θ) may be defined from the minor axis, with Φ as a toroidal angle. This choice of coordinates may give inaccurate results, since the resulting coordinate surfaces may not match, even in an approximate way, actual equilibrium magnetic surfaces. This has led us to the use of a (non-orthogonal) polar toroidal coordinate system $(r_t, \theta_t, \varphi_t)$ [30]. In the large aspect ratio limit $(A \gg 1)$ these coordinates reduce to the polar coordinates (r, θ, Φ). For arbitrary aspect ratio they may be defined in terms of the toroidal coordinates (ξ, ω, Φ) [31] by the following relations:

$$r_t = \frac{R_0'}{\cosh \xi - \cos \omega}, \tag{1}$$

$$\theta_t = \pi - \omega, \tag{2}$$

$$\varphi_t = \Phi, \tag{3}$$

where R_0' is the magnetic axis radius (defined as a degenerated magnetic surface of zero volume), different from R_0 by a small quantity called Shafranov shift. In Fig. 2 we depict some of the coordinate surfaces for this system, in the plane $\varphi = 0$, and (R, Z) are usual cylindrical coordinates.

The tokamak equilibrium magnetic field $\mathbf{B}_0$ is obtained from an ideal MHD static equilibrium model, described by the following equations [1,2,12]

$$\mathbf{J} \times \mathbf{B}_0 = \nabla p, \tag{4}$$

$$\nabla \times \mathbf{B}_0 = \mu_0 \mathbf{J}, \tag{5}$$

$$\nabla \cdot \mathbf{B}_0 = 0, \tag{6}$$

where p and $\mathbf{J}$ are the pressure and current density, respectively. We assume that the equilibrium field is axisymmetric, i.e., physical quantities of interest do not depend on the toroidal angle φ_t. Taking the dot product of (4) with $\mathbf{B}_0$ results in $\mathbf{B}_0 \cdot \nabla p = 0$, so that the magnetic field lies on constant pressure surfaces with the topology of closed tori. These magnetic surfaces may be also described by a poloidal flux $\Psi_p = \Psi_p(r_t, \theta_t)$ in such a way that

$$\mathbf{B}_0 \cdot \nabla \Psi_p = 0. \tag{7}$$

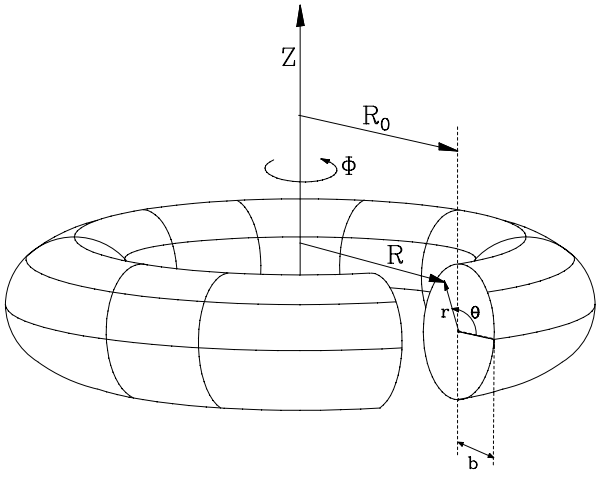

Fig. 1. Schematic diagram of a tokamak.

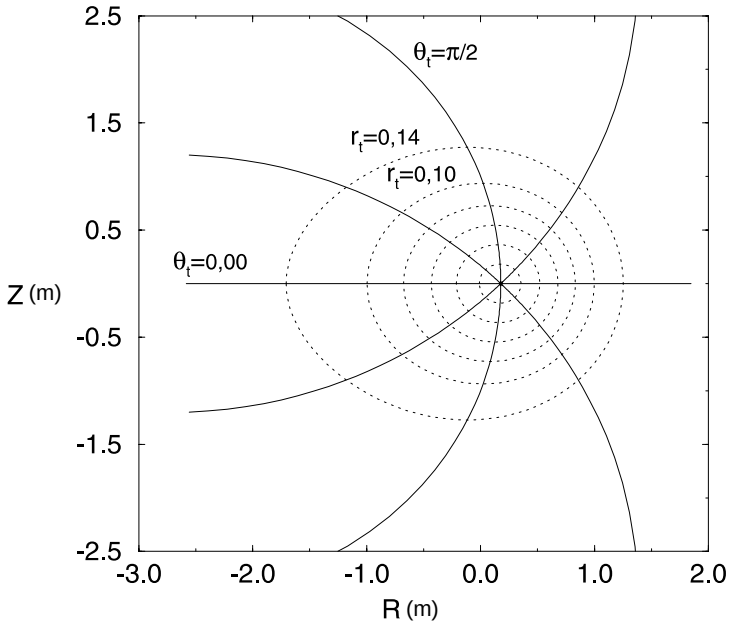

Fig. 2. Some coordinate surfaces of the polar toroidal coordinate system in the $\varphi = 0$ plane.

Another scalar function that is necessary to describe the equilibrium field is the poloidal current $I = I(r_t, \theta_t)$ satisfying

$$\mathbf{B}_0 \cdot \nabla I = 0. \tag{8}$$

The set of MHD Eqs. (4)–(6) may be shown to be equivalent, in the axisymmetric case, to a partial differential (Grad–Schlüter–Shafranov) equation involving the two scalar functions Ψ_p and I. In the polar toroidal coordinate system used in this work, this equation is written as [32]:

$$\frac{1}{r_t}\frac{\partial}{\partial r_t}\left(r_t\frac{\partial \Psi_p}{\partial r_t}\right)+\frac{1}{r_t^2}\frac{\partial^2 \Psi_p}{\partial \theta_t^2}=\mu_0 J_3(\Psi_p)+\mu_0 R_0'^2\frac{dp}{d\Psi_p}\left(2\frac{r_t}{R_0'}\cos\theta_t+\frac{r_t^2}{R_0'^2}\sin^2\theta_t\right)+\frac{r_t}{R_0'}\left[\cos\theta_t\left(2\frac{\partial^2\Psi_p}{\partial r_t^2}+\frac{1}{r_t}\frac{\partial\Psi_p}{\partial r_t}\right)+\sin\theta_t\left(\frac{1}{r_t^2}\frac{\partial\Psi_p}{\partial\theta_t}-\frac{2}{r_t}\frac{\partial^2\Psi_p}{\partial\theta_t\partial r_t}\right)\right], \tag{9}$$

where the toroidal current density is given by

$$J_3(\Psi_p) = -R_0'^2\frac{dp}{d\Psi_p}-\frac{d}{d\Psi_p}\left(\frac{1}{2}\mu_0 I^2\right). \tag{10}$$

The contravariant components of the equilibrium magnetic field, according to Eqs. (7) and (8), are

$$B_0^1 = -\frac{1}{R_0' r_t}\frac{\partial\Psi_p}{\partial\theta_t}, \tag{11}$$

$$B_0^2 = \frac{1}{R_0' r_t}\frac{\partial\Psi_p}{\partial r_t}, \tag{12}$$

$$B_0^3 = -\frac{\mu_0 I}{R^2}, \tag{13}$$

where

$$R^2 = R_0' 2\left[1-2\frac{r_t}{R_0'}\cos\theta_t-\left(\frac{r_t}{R_0'}\right)^2\sin^2\theta_t\right]. \tag{14}$$

We assume, at the large aspect ratio limit, that in lowest order the poloidal flux does not depend on θ_t, i.e., $\Psi_p(r_t)$. In this case, Eq. (9) reduces to an equilibrium equation similar to that obtained in a cylindrical geometry, but in terms of r_t [1]. The intersections of magnetic surfaces $\Psi_p(r_t) = \text{const.}$ with a toroidal plane are not concentric circles but present a Shafranov shift toward the exterior equatorial region [30]. Equilibrium magnetic surfaces are well-approximated by $r_t = \text{const.}$ coordinate surfaces.

The unknown function Ψ_p in Eq. (9) appears both as a dependent and independent variable. Hence, in order to seek a solution for Eq. (9) we need to assume profiles for both the pressure $p = p(\Psi_p)$ and current function $I = I(\Psi_p)$. In lowest order, however, there is another and easier way to proceed, since it is sufficient to assume a single spatial profile for the toroidal current density J_3, as it is already given by Eq. (10) in terms of p and I. We are free to choose any profile consistent with the boundary conditions to be adopted. In particular the plasma density must vanish at $r = a$, the plasma radius that is fixed by a material ring mounted inside the chamber. In this paper we adopt a peaked current profile, commonly observed in tokamak discharges [1,2], and given by

$$J_3(r_t) = \frac{I_p R_0'}{\pi a^2}(\gamma+1)\left(1-\frac{r_t^2}{a^2}\right)^{\gamma}, \tag{15}$$

where I_p is the total plasma current and γ is a positive constant.

An approximate solution for (9) may be sought expanding the poloidal flux Ψ_p in powers of the aspect ratio r_t/R_0'. The details of this calculation may be found in [28]. At lowest order the equilibrium field contravariant components are given by

$$B_0^1 = 0, \tag{16}$$

$$B_0^2 = \frac{\mu_0 I_p}{2\pi r_t^2}\left[1-\left(1-\frac{r_t^2}{a^2}\right)^{\gamma+1}\right], \tag{17}$$

$$B_0^3 = \frac{\mu_0 I_e}{2\pi R_0'^2}\left(1-2\frac{r_t}{R_0'}\cos\theta_t\right)^{-1}, \tag{18}$$

where $I_e \approx -2\pi I$ is the external current that generates the equilibrium toroidal field. Field lines spiral along the magnetic surfaces with a specific pitch characterized by a winding number, a term much used in Hamiltonian dynamics. In plasma physics its inverse, or safety factor, is more often used. If it has a rational (irrational) value, the corresponding surface is also called a rational (irrational) one. The name "safety factor" comes from plasma stability criteria involving the equilibrium field at the magnetic axis.

We define a poloidally averaged safety factor as

$$q(r_t) = \frac{1}{2\pi}\int_0^{2\pi}\frac{B_0^3(r_t,\theta_t)}{B_0^2(r_t,\theta_t)}\,d\theta_t \tag{19}$$

Using Eqs. (17) and (18) there results

$$q(r_t) = q_c(r_t)\left(1-4\frac{r_t^2}{R_0'^2}\right)^{-1/2}, \tag{20}$$

where

$$q_c(r_t) = \frac{I_e}{I_p}\frac{r_t^2}{R_0'^2}\left[1-\left(1-\frac{r_t^2}{a^2}\right)^{\gamma+1}\right]^{-1}, \tag{21}$$

We suppose that $q(0) = 1$, in order to avoid certain instabilities [1,2], so that it suffices to specify γ in order to have $q(a)$, so we choose $q(a) \approx 5$. In the numerical simulations to be described in this paper, we normalize the minor radius $b_t \equiv b$ and plasma radius a to the major radius R_0', so that $a/R_0' = 0.26$, $b_t/R_0' = 0.36$ [4]. Fig. 3(a) shows some equilibrium flux surfaces for this set of parameters, and Fig. 3(b) depicts the corresponding radial profile of the safety factor.

The design for the ergodic magnetic limiter to be considered here is essentially the same as in [28], and consists of N_a current rings of length ℓ located symmetrically along the toroidal circumference of the tokamak (Fig. 4). These current rings may be regarded as slices of a pair of external helical windings located at the tokamak minor radius $r_t = b_t$, conducting a current I_h in opposite senses for adjacent conductors. The role of these windings is to induce a resonant

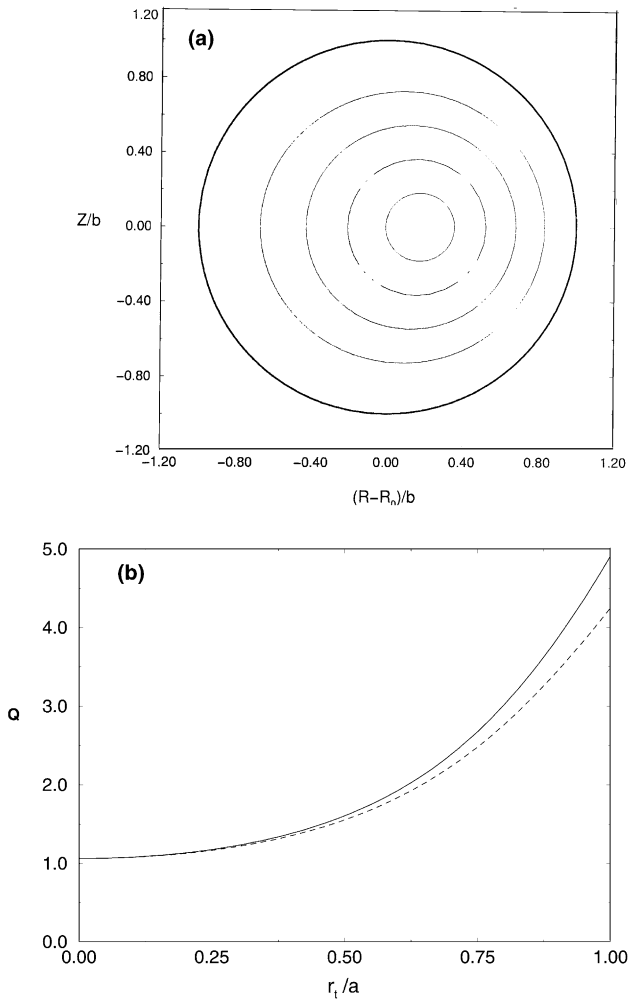

Fig. 3. (a) Equilibrium flux surfaces, and (b) safety factor radial profile for a tokamak.

perturbation in the tokamak, and to achieve this effect we must choose a helical winding with the same pitch as the field lines in the rational surface we want to perturb. Suppose that this surface have safety factor $q = m_0/n_0$, where m_0 and n_0 are positive integers. Hence the winding law must contain these two numbers. However, it should contain in addition a term expressing the helical field line pitch nonuniformity caused by the toroidal effect. So, we proposed the following winding law [28]

$$u_t = m_0(\theta_t + \lambda \sin\theta_t) - n_0\varphi_t = \text{constant}, \tag{22}$$

where λ is a parameter which value is dictated by the location of the main resonant magnetic surface to be destroyed, and where we aim to produce chaotic field lines. In our case, we choose the resonant effect to occur at the equilibrium rational magnetic surface with $q = 5$, since it is located near the plasma edge [see Fig. 3(b)], and corresponds to $\lambda = 0.54$.

The magnetic field produced by the resonant helical winding from which we build the EML rings is obtained by neglecting the plasma response and the penetration time through the tokamak wall. In this case, it is assumed to be a vacuum field $\mathbf{B}_L = \nabla \times \mathbf{A}_L$. In lowest order, the only non-vanishing component of $\mathbf{A}_L$ is [28]

$$A_{L3}(r_t, \theta_t, \varphi_t) = -\frac{\mu_0 I_h R_0'}{\pi} \sum_{k=-m_0}^{+m_0} J_k(m_0\lambda)\left(\frac{r_t}{b_t}\right)^{m_0+k} e^{i[(m_0+k)\theta_t - n_0\varphi_t]}, \tag{23}$$

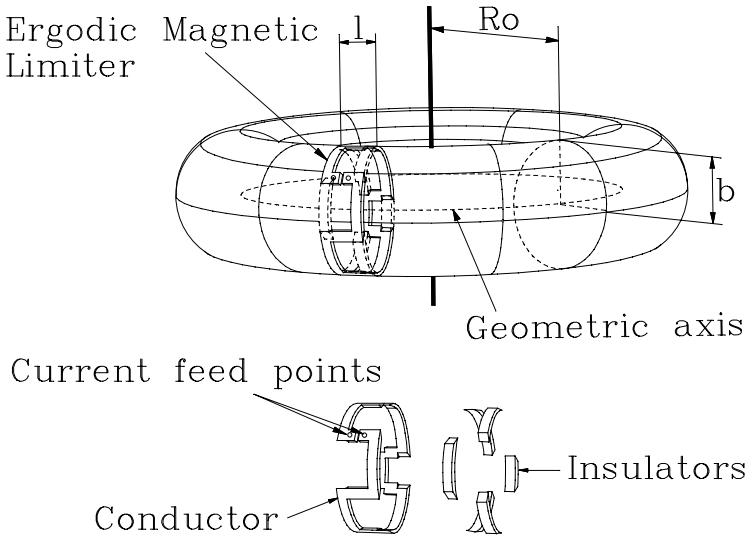

Fig. 4. Schematic diagram of an ergodic magnetic limiter.

The limiter field components are given by

$$B_{\mathrm{L}}^{1} = -\frac{1}{R_0' r_{\mathrm{t}}}\frac{\partial A_{\mathrm{L}3}}{\partial \theta_{\mathrm{t}}}, \tag{24}$$

$$B_{\mathrm{L}}^{2} = \frac{1}{R_0' r_{\mathrm{t}}}\frac{\partial A_{\mathrm{L}3}}{\partial r_{\mathrm{t}}} \tag{25}$$

and the model field will be the superposition: $\mathbf{B} = \mathbf{B}_0 + \mathbf{B}_{\mathrm{L}}$.

3. Derivation of the symplectic mapping

The magnetic field line equations $\mathbf{B} \times \mathbf{d}\ell = \mathbf{0}$, corresponding to the model fields described in the previous section, are written, using Eqs. (11)–(13), (24) and (25), as

$$\frac{\mathrm{d}r_{\mathrm{t}}}{\mathrm{d}\varphi_{\mathrm{t}}} = -\frac{1}{r_{\mathrm{t}} B_{\mathrm{T}}}\left(1 - 2\frac{r_{\mathrm{t}}}{R_0'}\cos\theta_{\mathrm{t}}\right)\frac{\partial}{\partial \theta_{\mathrm{t}}} A_{\mathrm{L}3}(r_{\mathrm{t}}, \theta_{\mathrm{t}}, \varphi_{\mathrm{t}}), \tag{26}$$

$$\frac{\mathrm{d}\theta_{\mathrm{t}}}{\mathrm{d}\varphi_{\mathrm{t}}} = \frac{1}{r_{\mathrm{t}} B_{\mathrm{T}}}\left(1 - 2\frac{r_{\mathrm{t}}}{R_0'}\cos\theta_{\mathrm{t}}\right)\frac{\partial}{\partial r_{\mathrm{t}}}\left[\Psi_{\mathrm{p}0}(r_{\mathrm{t}}) + A_{\mathrm{L}3}(r_{\mathrm{t}}, \theta_{\mathrm{t}}, \varphi_{\mathrm{t}})\right], \tag{27}$$

where $B_{\mathrm{T}} \equiv -\mu_0 I / R_0'$ is the toroidal magnetic field at the magnetic axis.

Since the equilibrium field is axisymmetric, we may set the angle $\varphi_{\mathrm{t}} = t$ as a time-like variable, and put field line Eqs. (26) and (27) in a Hamiltonian form

$$\frac{\mathrm{d}\mathscr{J}}{\mathrm{d}t} = -\frac{\partial H}{\partial \vartheta}, \tag{28}$$

$$\frac{\mathrm{d}\vartheta}{\mathrm{d}t} = \frac{\partial H}{\partial \mathscr{J}}, \tag{29}$$

where $(\mathscr{J}, \vartheta)$ are the action–angle variables of a Hamiltonian system. If H does not depend on φ, due to the axisymmetry, the equilibrium magnetic field configuration is a one-degree-of-freedom system, hence integrable in the Liouville sense. We may calculate the action $(\mathscr{J})$ and angle (ϑ) variables for this problem by defining:

$$\mathscr{J}(r_{\mathrm{t}}) = \frac{1}{2\pi R_0' B_{\mathrm{T}}}\int\int B_0^3(r_{\mathrm{t}}, \theta_{\mathrm{t}}) r_{\mathrm{t}}\,\mathrm{d}r_{\mathrm{t}}\,\mathrm{d}\theta_{\mathrm{t}} = \frac{1}{4}\left[1 - \left(1 - 4\frac{r_{\mathrm{t}}^2}{R_0'^2}\right)^{1/2}\right], \tag{30}$$

$$\vartheta(r_{\mathrm{t}}, \theta_{\mathrm{t}}) = \frac{1}{q(r_{\mathrm{t}})}\int_0^{\theta_{\mathrm{t}}} \frac{B_0^3(r_{\mathrm{t}}, \theta_{\mathrm{t}})}{B_0^2(r_{\mathrm{t}}, \theta_{\mathrm{t}})}\,\mathrm{d}\theta = 2\arctan\left[\frac{1}{\Omega(r_{\mathrm{t}})}\left(\frac{\sin\theta_{\mathrm{t}}}{1 + \cos\theta_{\mathrm{t}}}\right)\right], \tag{31}$$

where B_0^2 and B_0^3 are given by (17) and (18), respectively, and

$$\Omega(r_t) = \left(1 - 2\frac{r_t}{R_0'}\right)^{1/2}\left(1 + 2\frac{r_t}{R_0'}\right)^{-1/2}, \tag{32}$$

The addition of the magnetic field produced by a resonant helical winding characterized by Eq. (23) may be regarded as a Hamiltonian perturbation, so that we write

$$H(\mathscr{J},\vartheta,t) = H_0(\mathscr{J}) + H_1(\mathscr{J},\vartheta,t)\frac{1}{B_T R_0'^2}\left[\Psi_{p0}(\mathscr{J}) + A_{L3}(\mathscr{J},\vartheta,t)\right]. \tag{33}$$

The perturbing Hamiltonian, characterizing the EML field, may be expanded in the action–angle variables of the equilibrium field as:

$$H_1(\mathscr{J},\vartheta,t) = \sum_{m'=0}^{2m_0} H_{m'}(r_t(\mathscr{J}))e^{i[m'\theta_t(\mathscr{J},\vartheta)-n_0 t]}, \tag{34}$$

where

$$H_{m'}(r_t) = -J_{m'-m_0}(m_0\lambda)\left(\frac{r_t}{b_t}\right)^{m'}. \tag{35}$$

These expressions may be conveniently rewritten as

$$H_1(\mathscr{J},\vartheta,t) = \sum_{n=0}^{2m_0} H_n^*(\mathscr{J})e^{i(m\vartheta-n_0 t)}, \tag{36}$$

with

$$H_m^*(\mathscr{J}) = \sum_{m'=0}^{2m_0} H_{m'}(r_t(\mathscr{J}))S_{m,m'}(\mathscr{J}), \tag{37}$$

where the numerical coefficients are given by

$$S_{m,m'}(\mathscr{J}) = (-1)^m\left(\frac{c_1(\mathscr{J})}{c_2(\mathscr{J})}\right)^{m+m'}\sum_{n=0}^{m}(-1)^n\alpha_n(m,m')\left(\frac{c_1(\mathscr{J})}{c_2(\mathscr{J})}\right)^{-2n}, \tag{38}$$

with

$$c_1(\mathscr{J}) = 1 - \frac{1}{\Omega(r_t(\mathscr{J}))}, \tag{39}$$

$$c_2(\mathscr{J}) = 1 + \frac{1}{\Omega(r_t(\mathscr{J}))}, \tag{40}$$

$$\alpha_n(m,m') = \begin{cases} 1 & \text{if } m = 0 \quad \text{and} \quad n = 0, \\ m' & \text{if } m = 1 \quad \text{and} \quad n = 0 \text{ or } n = 1, \\ m'\frac{(m+m'-n-1)!}{(m-n)!(m'-n)!n!} & \text{if } m > 1 \quad \text{and} \quad n \leqslant m', \\ 0 & \text{if } m > 1 \quad \text{and} \quad n > m'. \end{cases} \tag{41}$$

This treatment, however, does not include the effect of the finite length ℓ of each EML ring, which is typically a small fraction of the total toroidal circumference $2\pi R_0'$. This introduces a time-dependent term which explicitly breaks the integrability of the configuration. If ℓ is small enough, we can model its effect as a sequence of delta-functions centered at each ring position [27]:

$$H_L(\mathscr{J},\vartheta,t) = H_0(\mathscr{J}) + \frac{\ell}{R_0'}H_1(\mathscr{J},\vartheta,t)\sum_{k=-\infty}^{+\infty}\delta\left(t - k\frac{2\pi}{N_a}\right), \tag{42}$$

where the N_a rings are symmetrically distributed in the toroidal direction.

We can derive, due to the impulsive perturbation, a stroboscopic map for field line dynamics, by defining $\mathscr{J}_n$ and ϑ_n as the action and angle variables just after the nth kick due to a limiter ring at the toroidal positions $\varphi_k = 2k\pi/N_a$, with $k = 0, 1, \ldots, N_a - 1$ [26]. The (area-preserving) mapping for this near-integrable system is [14]

$$\mathscr{J}_{n+1} = \mathscr{J}_n + \epsilon f(\mathscr{J}_{n+1}, \vartheta_n, t_n), \tag{43}$$

$$\vartheta_{n+1} = \vartheta_n + \frac{2\pi}{N_a q(\mathscr{J}_{n+1})} + \epsilon g(\mathscr{J}_{n+1}, \vartheta_n, t_n), \tag{44}$$

$$t_{n+1} = t_n + \frac{2\pi}{N_a}, \tag{45}$$

where

$$f(\mathscr{J}, \vartheta, t) = -\frac{\partial H_1(\mathscr{J}, \vartheta, t)}{\partial \vartheta}, \tag{46}$$

$$g(\mathscr{J}, \vartheta, t) = \frac{\partial H_1(\mathscr{J}, \vartheta, t)}{\partial \mathscr{J}}, \tag{47}$$

and the perturbation parameter is

$$\epsilon = -2\left(\frac{\ell}{2\pi R_0'}\right)\left(\frac{I_h}{I}\right). \tag{48}$$

which is usually small, since in experiments we have $\ell \ll 2\pi R_0'$ and $I_h \ll I$.

4. Pendular islands

In this section we will study the effect of resonances caused by the magnetic field produced by an ergodic limiter. In the phase space the exact resonance will be the center of a magnetic island with pendular shape. In order to use standard results of perturbation theory we have to start from an expansion of the perturbing Hamiltonian in modes related to the angles ϑ and t. The Hamiltonian for the tokamak with ergodic limiters, Eq. (42), may be rewritten by Fourier-expanding the periodic delta function, in the following form

$$H_L(\mathscr{J}, \vartheta, t) = H_0(\mathscr{J}) + \tilde{\epsilon} \sum_{m=0}^{2m_0} \sum_{s=-\infty}^{+\infty} H_m^*(\mathscr{J}) e^{i[m\vartheta - (n_0 + sN_a)t]}, \tag{49}$$

where the small parameter is redefined here as

$$\tilde{\epsilon} = -\frac{I_h \ell N_a}{2\pi^2 I R_0'} = \frac{N_a}{2\pi}\epsilon. \tag{50}$$

Perturbative treatments of the Hamiltonian (49) present divergences at resonances, for which the phase is stationary: $d\vartheta/dt = n/m$, with $n \equiv n_0 + sN_a$ for some pair of integers (m, n). This is equivalent to find a rational magnetic surface with safety factor m/n that resonates with some harmonic of the perturbing field. Let us choose $m = m_0$ and $s = 0$, or $n = n_0$, in such a way that (m_0, n_0) characterizes a rational surface in the periphery of the tokamak column. By inspecting Fig. 3(b) we find that $(m_0, n_0) = (4, 1)$ or $(5, 1)$ are suitable for our purposes, since the corresponding surfaces are located in the region comprising the plasma edge and the tokamak inner wall, where chaotic dynamics is expected to take place.

Hence, we consider the Hamiltonian in the neighborhood of the action $\mathscr{J} = \mathscr{J}_0$ for which the safety factor is m_0/n_0. Expanding the unperturbed Hamiltonian H_0 up to quadratic terms, and taking only the resonant term from the perturbing Hamiltonian H_1, we have

$$H \approx H_0(\mathscr{J}_0) + \left.\frac{dH_0}{d\mathscr{J}}\right|_{\mathscr{J}=\mathscr{J}_0} \Delta\mathscr{J} + \frac{1}{2}\left.\frac{d^2H_0}{d\mathscr{J}^2}\right|_{\mathscr{J}=\mathscr{J}_0} (\Delta\mathscr{J})^2 + \tilde{\epsilon} H_{m_0}^*(\mathscr{J}_0) e^{i(m_0\vartheta - n_0 t)}, \tag{51}$$

where $\Delta\mathscr{J} = \mathscr{J} - \mathscr{J}_0$.

The standard procedure [14] for removing the (m_0, n_0) resonant term is to go to a rotating frame through a canonical transformation of variables $(\mathscr{J}, \vartheta) \to (\mathscr{J}', \vartheta')$ performed by means of the following time-dependent generating function

$$G(\Delta\mathscr{J}', \vartheta, t) = (m_0\vartheta - n_0 t)\Delta\mathscr{J}' \tag{52}$$

resulting in the relations: $\Delta\mathscr{J}' = \Delta\mathscr{J}/m_0$, $\vartheta' = m_0\vartheta - n_0 t$, and $H' = H - (n_0/m_0)\Delta\mathscr{J}$. The Hamiltonian in the neighborhood of the resonance is written as

$$H'(\Delta\mathscr{J}', \vartheta') = \frac{1}{2} W(\Delta\mathscr{J}')^2 - \tilde{\epsilon} K \cos\vartheta', \tag{53}$$

which is the pendulum Hamiltonian with constants given by

$$W = m_0^2 \left.\frac{\mathrm{d}^2 H_0}{\mathrm{d}\mathscr{J}^2}\right|_{\mathscr{J}=\mathscr{J}_0}, \tag{54}$$

$$K = -H^*_{m_0}(\mathscr{J}_0). \tag{55}$$

In the phase space $(\Delta\mathscr{J}', \vartheta')$ the pendulum libration (closed) curves define a magnetic island, whose half-width is given by the maximum libration amplitude, given by

$$\Delta\mathscr{J}'_{\max} = 2\left(\tilde{\epsilon}\left|\frac{K}{W}\right|\right)^{1/2}. \tag{56}$$

The frequency of the pendulum small librations around the exact resonance at $(\Delta\mathscr{J}' = 0, \vartheta' = 0)$ is

$$\omega'_0 = (\tilde{\epsilon}|KW|)^{1/2}. \tag{57}$$

In this approximation the island width and frequency are proportional to $\sqrt{\tilde{\epsilon}} \sim \sqrt{I_\mathrm{h}/I_\mathrm{p}}$.

Now, we present numerical results for an ergodic magnetic limiter with $(m_0, n_0) = (4, 1)$ and $\lambda = 0.48$. Fig. 5(a) shows a large number of orbits obtained from different initial conditions of the symplectic mapping (43)–(45) for the

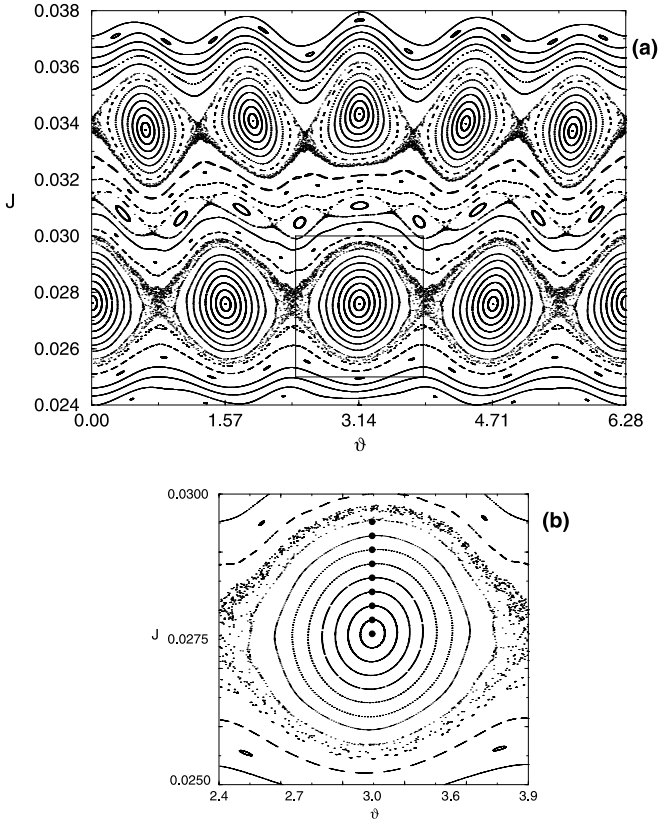

Fig. 5. (a) Phase portrait, in action–angle variables, for a tokamak with $q(0) = 1$, $q(a) = 5$, and an ergodic limiter with $(m_0, n_0) = (4, 1)$, $\lambda = 0.48$, and $I_\mathrm{h} = 0.81\%$ of I_p; (b) enlargement of an island of the 4:1 chain, with indication of the initial conditions there used.

case in which the limiter current I_h is 0.81% of the total plasma current I_p. We may see a chain of four magnetic islands (a 4:1 chain, with one of their islands being magnified in Fig. 5(b)) located at $\mathscr{J}_0 \approx 0.027$, and other satellite islands, among which a reasonably large 5:1 chain centered at 0.034. In Fig. 6 we plot the island half-width and frequency versus the limiter current for the same parameters as in Fig. 5. The black dots are estimated on the numerically obtained phase portraits like Fig. 5(a), whereas the solid lines are the theoretical predictions of Eqs. (56) and (57). Whereas for small limiter currents the agreement is good, for higher values of I_h there is a small but almost constant difference between the numerical and theoretical values. This is explained by the increasing difficulty in determining the boundary of an island when it has got a chaotic region in the vicinity of its separatrix.

A different way to characterize the magnetic surfaces consists on following some orbit in the phase space, tracking for example its ϑ-coordinate, and performing a power spectrum analysis of its frequencies. Fig. 7 shows such a result for a non-chaotic orbit picked up from Fig. 5(a). We call $\omega_{S_{\max}}$ the frequency of the highest peak in the power spectrum density. It turns out that $\omega_{S_{\max}}$ is nothing but the inverse of safety factor $1/q$ of the magnetic surface on which this orbit lies, as confirmed by Fig. 8, where the sampling frequency is $\omega_A = 1$, and many different non-chaotic orbits inside an island are tested. The other peaks result from a large number of combinations of harmonics and sub-harmonics, as is typical in quasi-periodic orbits on KAM tori [14]. On the other hand, chaotic orbits correspond to destroyed magnetic surfaces and do not present a well-defined frequency or safety factor.

When we consider these time series for points inside a given magnetic island, the libration frequency is, in general, different from that around resonance ω_0'. For a m_0/n_0 island the sampling frequency is $\omega_A = 1/m_0$ so that $\omega_{\text{in}} = m_0\omega_{S_{\max}} = 1/q_{\text{in}}$, where q_{in} is the safety factor of the tori inside an island. Fig. 9 shows numerical results for ω_{in} in various points inside the 4:1 island depicted in Fig. 5(b). The frequency decreases to zero as we approach the separatrix, as is also predicted in an exact calculation made with the help of elliptic functions [14].

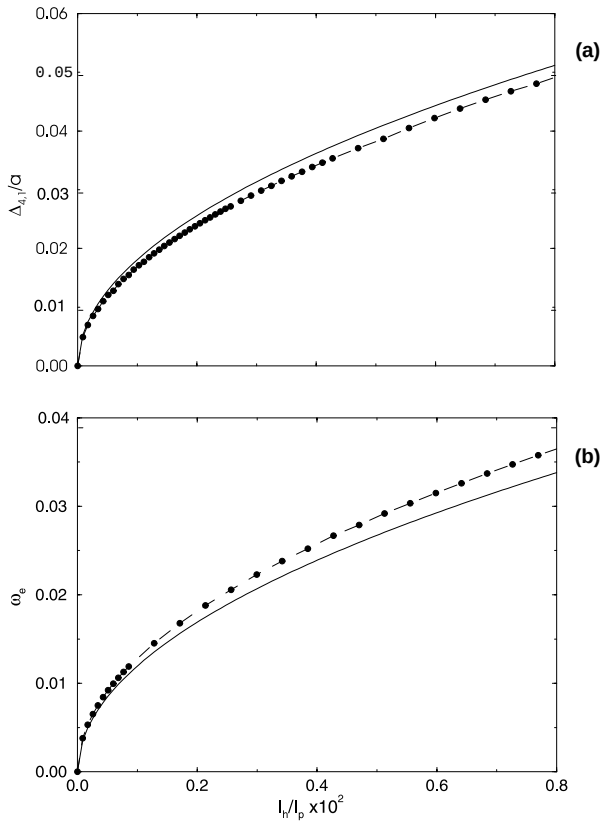

Fig. 6. (a) Half-width and (b) frequency at the center of a 4:1 island, in terms of the limiter current. The remaining parameters are the same as in Fig. 5. Dots are values estimated from phase portraits and the solid curves are obtained from Eqs. (56) and (57).

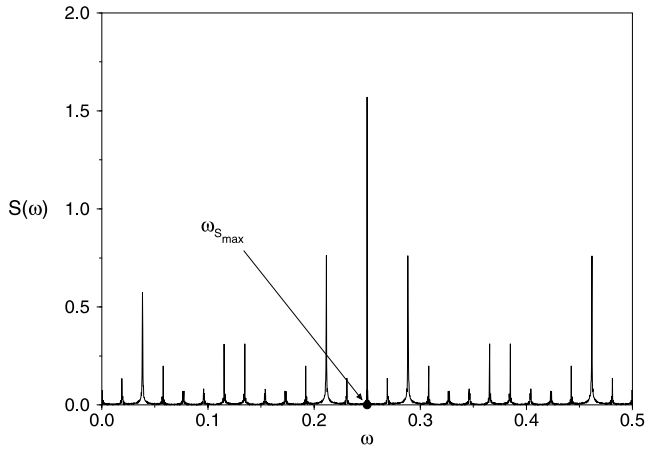

Fig. 7. Power spectral density of frequencies for the time series of the ϑ-coordinate of orbit points taken from the island depicted in Fig. 5(b).

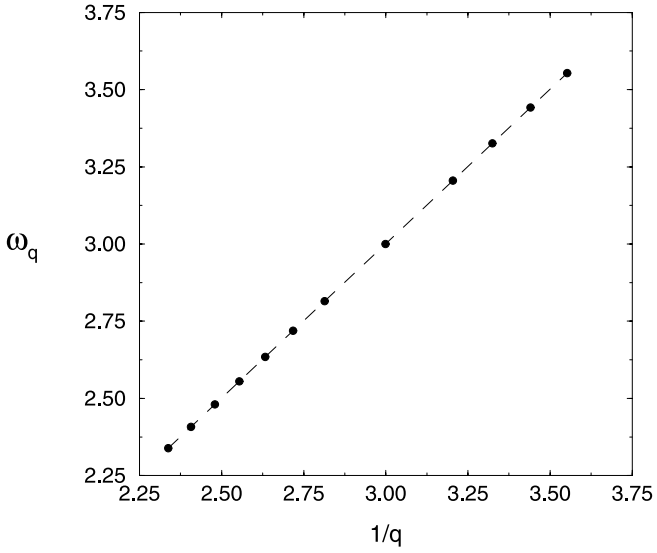

Fig. 8. Frequency of the highest power spectral peak in terms of the corresponding safety factor.

5. Onset of chaos

The fate of the equilibrium magnetic surfaces, after a perturbation breaks the system integrability, is basically determined by their safety factors. KAM theory predicts that, for those irrational surfaces with safety factors sufficiently far from a rational m:n, the topology is preserved, and the surfaces are only slightly deformed from the unperturbed tori (KAM surfaces) [14]. On a rational surface and in a neighborhood about it the KAM theorem fails, and we have to resort to the Poincaré–Birkhoff theorem.

Consider the field line mapping (43)–(45) in the absence of perturbation ($\epsilon = 0$). The toroidal magnetic surfaces are invariant circles in the Poincaré surface of section (for the time-$2\pi/N_a$ map), each of them characterized by a safety factor $q(r_t(\mathscr{J}))$. If it is a rational surface, then any point on the invariant circle $q(\mathscr{J}) = m/n$ is a period-n fixed point of the mapping. According to the Poincaré–Birkhoff theorem there exists an even number ($2kn$, with $k = 1, 2, \ldots$) of fixed points that remain after the perturbation. Half of them are elliptic (linearly stable), with closed trajectories encircling them, and the other half are hyperbolic (linearly unstable). Successive hyperbolic points are connected by a separatrix,

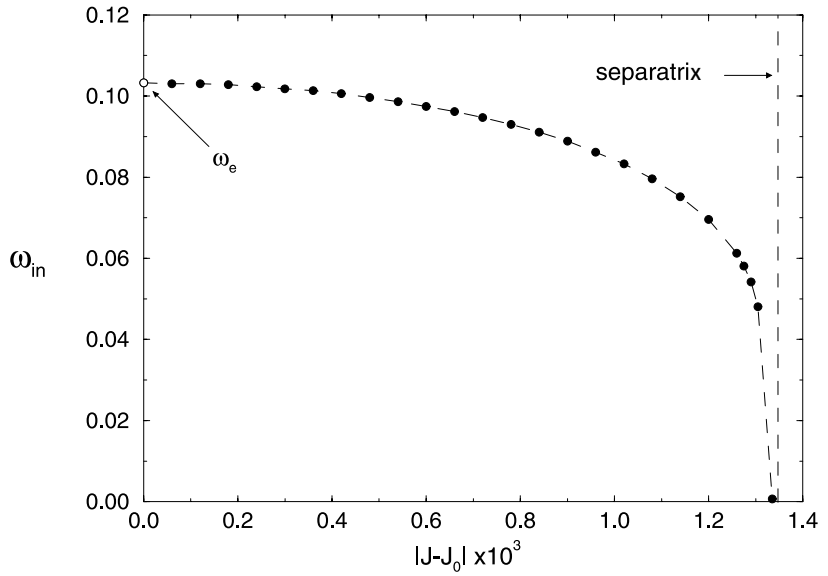

Fig. 9. Frequency of librations inside a 4:1 island versus the value of the action variable.

repeating the pendulum Hamiltonian pattern. In other words, rational surfaces disappear under the perturbation leaving an even number of fixed points, around which there exists an island chain.

There is a crucial difference, however, since for a pendulum the separatrices smoothly join adjacent hyperbolic points, and for a near-integrable system (ϵ small) this is no longer true. The unstable manifold leaving one hyperbolic point intersects the stable manifold arriving at the neighboring hyperbolic point. If the latter is topologically the same point as the former, the intersection is called a homoclinic point; otherwise is a heteroclinic intersection. If a single intersection occurs, there are infinitely many such intersections, leaving a sequence of homoclinic points. Since the areas enclosed by the intersections are mappings of one another, these areas are preserved and as successive crossings become closer, the unstable and stable manifolds have to oscillate more wildly. The region near the separatrix, where the homoclinic or heteroclinic points are abundant, is characterized by the absence of KAM surfaces and it shows chaotic motion. For sufficiently small perturbations, however, this chaotic behavior occurs in regions bounded by KAM surfaces, that act as dikes, preventing large-scale chaotic diffusion. These regions of local separatrix chaos grow as the perturbation amplitude increases. We expect a barrier transition to global field line chaos if this amplitude exceeds a critical value.

These two situations are illustrated in Figs. 10 and 11, where we present phase portraits of a large number of orbits, when the perturbation amplitude – which turns out to be the normalized limiter current – is increased past a critical value. Fig. 10, obtained when the limiter current is 1.1% of the plasma current, shows two adjacent island chains (4:1 and 5:1) with small chaotic regions restricted to the neighborhood of their separatrices and hyperbolic points. Many KAM surfaces remain between these chains, as well as many higher-order resonances with their own locally chaotic regions. Increasing the limiter current to 1.4% of the plasma current (Fig. 11) is sufficient to destroy all the KAM surfaces between the 4:1 and 5:1 chains and make the locally chaotic regions of these two resonances to overlap. This yields a large-scale chaotic region, where the excursion of chaotic field lines is larger than before, since it spans more than two times the width of each island.

The question of the onset of global or large-scale chaos has been investigated in depth for $1\frac{1}{2}$ degree of freedom near integrable systems. Sophisticated methods, as the renormalization scheme [33], or the residue technique [34], can determine with great accuracy the threshold for destruction of the last KAM surface between two neighbor resonances. Good results (within the experimental accuracy) can be obtained by using simpler methods, as the modified Chirikov criterion [14]. In its original version, this criterion prescribes the touching of neighbor separatrices in order to achieve global Hamiltonian chaos [35]. However, it turns out that this is an overestimation of the necessary perturbation strength, since the locally chaotic regions overlap before the separatrices themselves.

Hence, empirical rules, as the "two-thirds" rule, have been proposed in order to take this fact into account without modifying the simple form of the Chirikov criterion [14]. However, it turns out that even this rule is not always a useful tool, since it holds for pairs of islands of similar widths, which is not the case for the perturbation

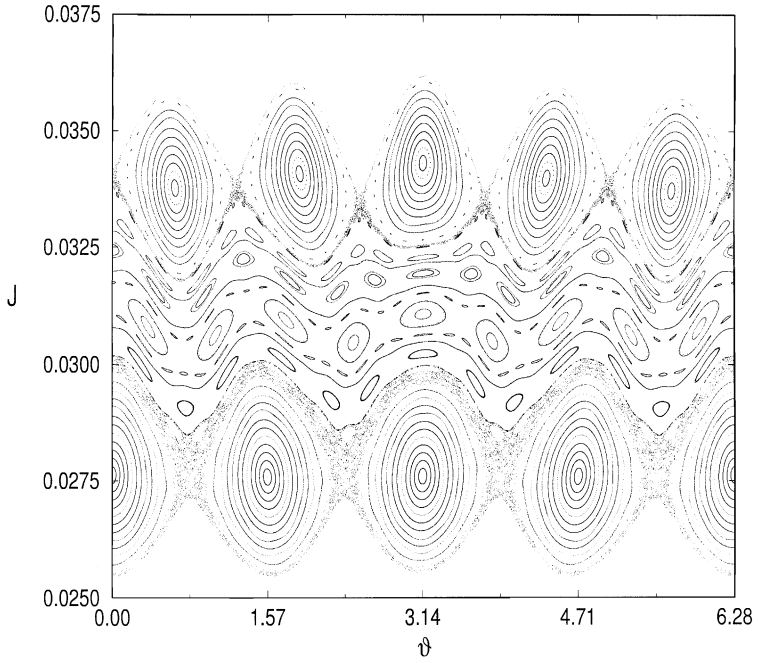

Fig. 10. Phase portrait, in action–angle variables, for a tokamak with $q(0) = 1$, $q(a) = 5$, and an ergodic limiter with $(m_n, n_0) = (4, 1)$, $\lambda = 0.48$, and $I_h = 1.1\%$ of I_p.

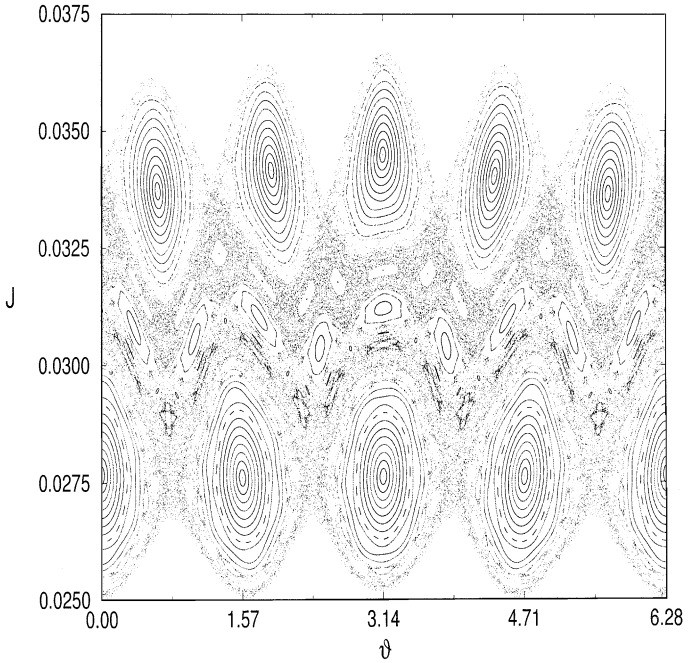

Fig. 11. Phase portrait, in action–angle variables, for a tokamak with $q(0) = 1$, $q(a) = 5$, and an ergodic limiter with $(m_n, n_0) = (4, 1)$, $\lambda = 0.48$, and $I_h = 1.4\%$ of I_p.

produced by an ergodic limiter, that makes islands thinner as we depart from the tokamak periphery. In this work, we advocate that a "four-fifths" rule would be more appropriate in this and other similar situations [27].

Bearing in mind these remarks, we define the following stochasticity parameter, according Chirikov to [35]

$$\chi = \frac{1}{2}\left[\frac{(\Delta\mathscr{J})_{4,1} + (\Delta\mathscr{J})_{5,1}}{|\mathscr{J}_{0,4} - \mathscr{J}_{0,5}|}\right], \tag{58}$$

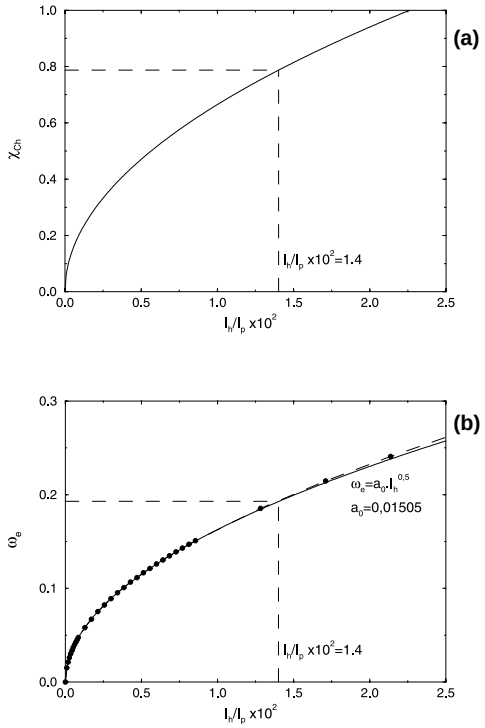

Fig. 12. (a) Stochasticity parameter of Chirikov, in terms of the limiter current. The critical current was taken to be the one related to a value of 4/5 for this parameter; (b) the same for the frequency in the center of the island.

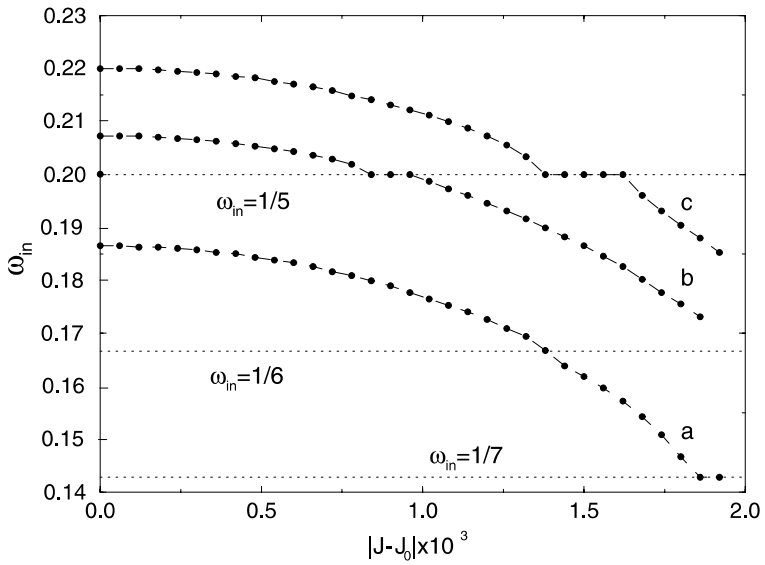

Fig. 13. Frequency of three closed orbits inside a 4:1 island versus the corresponding value of the action. The observed plateaus are due to secondary resonances therein.

where $\mathscr{J}_{m,n}$ are the half-widths of the island around a (m,n) resonance, and $\mathscr{J}_{0,m}$ are the location of the corresponding rational surfaces. The threshold for simple island overlap is given by $\chi = 1$, and the two-thirds and four-fifths rule correspond to critical values equal to $2/3$ and $4/5$, respectively. Fig. 12(a) depicts the behavior of the stochasticity parameter in terms of the limiter current. It indicates that – according to the latter criterion – the critical limiter current is about 1.4% of the plasma current, which is a reasonable value since it demands limiter currents of only hundreds of ampéres, for typical discharges of tens of kiloampéres in small tokamaks.

There is a universal relation between the critical value of the Chirikov parameter (58) to the safety factor q_e in the center of an island: $\chi_{\text{crit}} = 4/q_e$. It is universal in the sense that it holds for resonances of arbitrary higher order. The critical value for the limiter current we have just estimated corresponds to the appearance of a chain of five secondary islands, for which $q_e = 5/1$, in the midst of the primary island. This may be observed in Fig. 12(b), which shows the increase of the frequency at the center of a 4:1 island as a function of the limiter current. For $I_{\text{h}} \approx 1.4\%$ of I_{p} it turns out that $\omega_e \approx 0.2$.

The presence of secondary island chains may be also evidenced by computing the frequency ω_{in} inside a primary island, as depicted in Fig. 13, where this is done for the 4:1 primary chain and different values of the perturbation strength. The presence of plateaus in this figure indicates the existence of secondary islands in the midst of this primary island. Note that if a plateau does not show up it does not mean that there is no secondary island there, but only that we picked up insufficient orbits inside the island to evidence the secondary islands. In fact, their number is infinite, but most of them are too small to be distinguished in the phase portraits. Fig. 14 shows the corresponding phase portraits (only a small portion of the phase space containing the island is shown) for the three values of the limiter current considered in the previous figure.

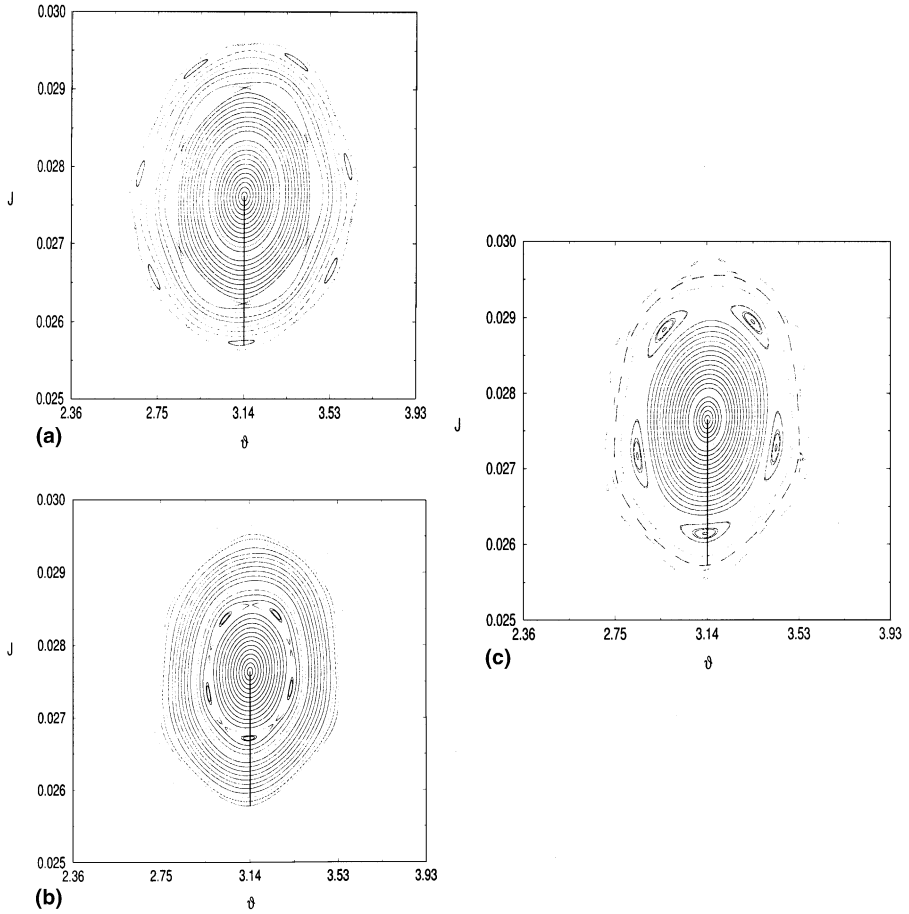

Fig. 14. Portions of the phase portrait, in action–angle variables, for an ergodic limiter with $(m_n, n_0) = (4,1)$, $\lambda = 0.48$, and: (a) $I_{\text{h}} = 1.3\%$ of I_{p}; (b) 1.6% of I_{p}; (c) 1.8% of I_{p}. These cases are taken from the curves of Fig. 13.

Since the frequency in the center of the primary island increases with the limiter current, according to Eq. (57), the secondary island chain that appears follows a decreasing sequence for their safety factor. For example, if a 7/1 secondary chain is observed for a given limiter current, islands with 6/1, 5/1, etc. will appear if the perturbation strength increases. The secondary island that already exist are pushed toward the primary island separatrix. In Fig. 14 we see that the 6/1 secondary chain migrates in this way as we increase I_h from 1/3% to 1.8% of I_p.

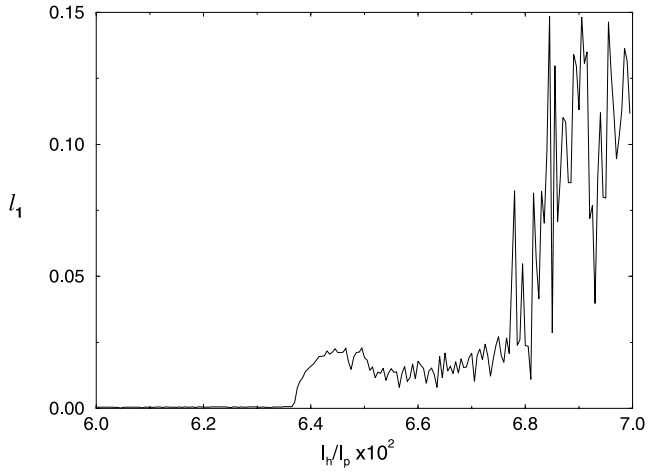

Fig. 15. Lyapunov exponent of an orbit picked up from the center of a 4:1 island, as a function of the limiter current.

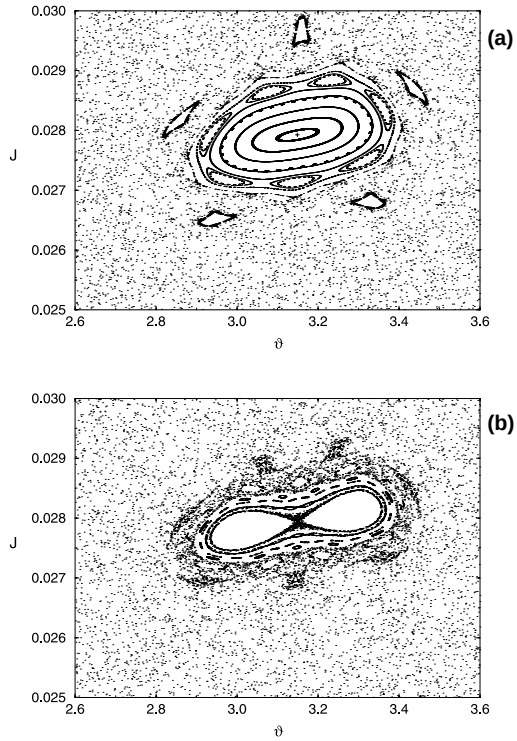

Fig. 16. Portions of the phase portrait, in action–angle variables, for an ergodic limiter with $(m_n, n_0) = (4, 1)$, $\lambda = 0.48$, and: (a) $I_h = 6.3\%$ of I_p; (b) 6.7% of I_p.

6. Bifurcation phenomena

As the current limiter builds up, new phenomena are expected to appear, besides the enlargement of the locally chaotic regions in the neighborhood of the islands' separatrices [14,36]. Let us fix our attention on the center of a

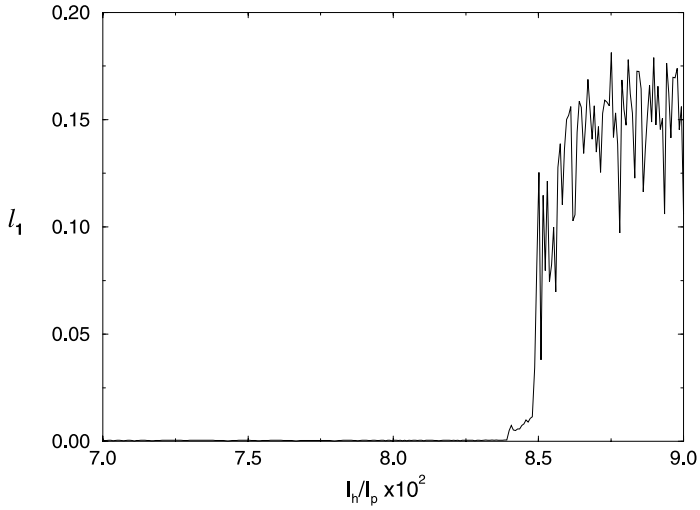

Fig. 17. Lyapunov exponent of an orbit picked up from the center of the 8:1 island as a function of the limiter current.

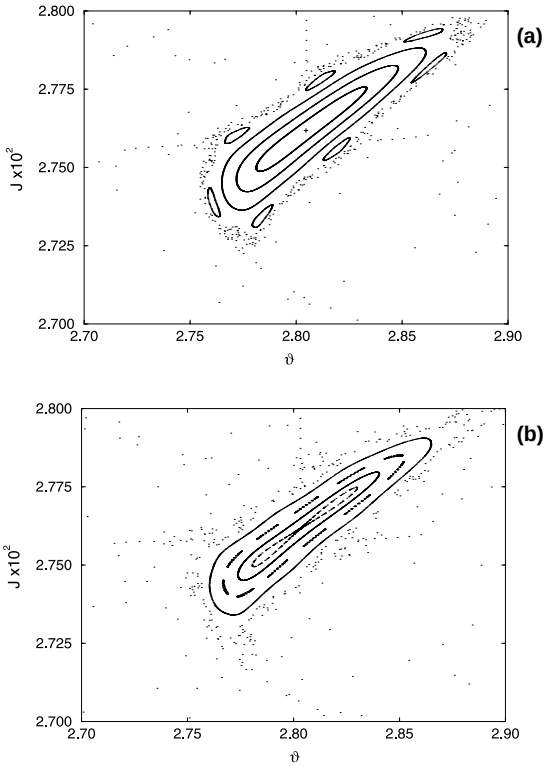

Fig. 18. Portions of the phase portrait, in action–angle variables, for an ergodic limiter with $(m_n, n_0) = (4, 1)$, $\lambda = 0.48$, and: (a) $I_h = 8.3\%$ of I_p; (b) 8.4% of I_p.

primary island chain, where there exists a stable fixed point of the field line mapping. For example, the centers in a 4:1 chain are periodic points of a stable period-4 orbit. As the limiter current is further increased, it may happen that this periodic orbit looses its stability and a new stable periodic orbit with period-8 appears, configuring a period-doubling Hamiltonian bifurcation.

Let us follow an orbit starting very close to one of these elliptic period-4 points and compute the corresponding maximal Lyapunov exponent, using the Ruelle–Eckmann algorithm [37]. The results for many values of the limiter current are shown in Fig. 15. For $I_h \approx 6.37\%$ of the plasma current this orbit loses stability and becomes an unstable saddle point. This unstable orbit belongs to a chaotic region, since the Lyapunov exponent has become positive.

In order to visualize the bifurcation that has occurred there, in Figs. 16(a) and (b) we show portions of the phase portrait that focuses on the evolution of the center of this period-4 orbit as I_h builds up. For $I_h = 6.3\%$ of I_p this orbit is still stable [Fig. 16(a)], whereas for 6.7% it became unstable and two new stable orbits appear in its neighborhood. From the field line point of view these newborn stable orbits represent magnetic axes that are formed for these extremely high perturbation amplitudes. This phenomenon has been previously been described in the fusion literature [38,39]. Note that from Fig. 16(b) that the two newborn stable orbits are centers of island-shaped structures, and that the orbit that lost its stability is now an unstable saddle in the midst of a locally chaotic region near the separatrices of new island-shaped structures. This explains the positive values of the Lyapunov exponent that we have observed in Fig. 15.

We were able to observe a second period-doubling bifurcation related to the centers of a period-8 chain. As the limiter current is further increased we observe the jump of the corresponding Lyapunov exponent (Fig. 17) for $I_h \approx 8.35\%$ of I_p. The loss of stability of the period-8 orbit and the appearance of a stable period-16 orbit is depicted in Figs. 18(a) and (b), for limiter currents slightly under and above this bifurcation value, respectively.

Area-preserving maps as Eqs. (43)–(45) present period-doubling bifurcations, but with some important differences when compared with their dissipative counterparts [14]. Even though the period-doubling cascade is expected to have an accumulation point, with the distances between successive bifurcations decreasing geometrically, the characteristic exponents are different from those of dissipative two-dimensional maps [40].

7. Conclusions

In this paper we derived a symplectic mapping to follow magnetic field lines in a tokamak with an ergodic magnetic limiter. The advantages of our procedure are: (a) we adopted a coordinate system which naturally embodies the plasma toroidal configurations [1,2,12]; (b) model fields were derived from sound physical assumptions: the equilibrium fields were not introduced in an ad hoc fashion [25,26], but came from the solution of an MHD equilibrium set of equations; (c) the limiter field was obtained from a direct calculation, assuming an impulsive character in order to make possible to obtain an analytical mapping. With the equations obtained, it it feasible to follow a very large number of orbits using less computer time than the symplectic integration of ordinary differential equations for field lines. This is particularly important if one is interested in the long-time behavior of field lines, as in studies of field line diffusion and loss due to collisions with the tokamak wall [29].

We obtained an explicit form of a Hamiltonian for the equilibrium field, with the ergodic limiter effect being considered a near-integrable perturbation. The canonical equations from this Hamiltonian were integrated to obtain a mapping. We remark that there is no rigorous derivation of the map (43)–(45) from the Hamiltonian function (42) because the integration along the delta functions is not well-defined. A general perturbative procedure for the construction of symplectic maps in Hamiltonian systems of the type (42) has been recently developed [21,41]. On the other hand, our map satisfies some necessary constraints [22]: (i) it is symplectic in the sense that the Hamiltonian structure of the field line equations is reflected in the map, since it is written in terms of action–angle variables; and (ii) it is compatible with toroidal geometry, since our action variable $\mathscr{J}$ is always a non-negative number, i.e., a field line starting on the magnetic axis may either remain on the axis or move to a positive $\mathscr{J}$, but never to a negative $\mathscr{J}$. We stress that the second condition is not fulfilled by the Chirikov–Taylor standard map [35], for example.

Using a secular perturbation technique we obtained the widths and locations of the primary islands due to resonances between the perturbing limiter field and the equilibrium tokamak field. Theoretical results are in good agreement with numerical results obtained by using our mapping. A detailed analysis of the frequencies of orbits inside a primary islands gave information about the appearance of secondary and higher-order islands. The onset of chaos due to the interaction of neighbor island chains was investigated through the use of a modified Chirikov criterion, taking into account that the creation of a large region of chaotic field lines occurs before the primary islands' separatrices touch each other. A "four-fifths" rule was found sufficient to yield a reliable value for the barrier transition to global chaos. For the interaction of a 4:1 and a 5:1 resonance (which would generate such a region in the outer plasma column) we

found that the critical limiter current is 1.4% of the plasma current. This is a reasonable value, taking into account the technical requirements for the operation of an ergodic limiter.

As the limiter current is further increased, even the center of an island may become unstable and bifurcate into two new stable points, which correspond to newborn magnetic axes. We were able to follow two of such period-doubling bifurcations, what suggests a cascade of accumulating bifurcations. Further work is still needed to determine the accumulation rates and compare them to the universal values theoretically predicted for area-preserving two-dimensional mappings.

Acknowledgements

This work was made possible with partial financial support of the following agencies: CNPq (Conselho Nacional de Desenvolvimento Científico e Tecnológico), CAPES (Coordenação de Aperfeiçoamento de Pessoal de Nível Superior), FAPESP (Fundação de Amparo à Pesquisa do Estado de São Paulo) , and Fundação Araucária (State of Paraná, Brazil).

References

[1] Freidberg JP. Ideal magnetohydrodynamics. New York: Plenum Press; 1987.
[2] Wesson J. Tokamaks. Oxford: Oxford University Press; 1987.
[3] Morrison PJ. Magnetic field lines, Hamiltonian dynamics and nontwist systems. Phys Plasmas 2000;7:2279.
[4] Wootton AJ, Carreras BA, Matsumoto H, McGuire K, Peebles WA, Ritz ChP, et al. Fluctuations and anomalous transport in tokamaks. Phys Fluids B 1990;2:2879.
[5] Wagner F, Stroh U. Transport in toroidal devices – the experimentalist's view. Plasma Phys Controlled Fusion 1993;35:1321.
[6] McCool S et al. Electron thermal confinement studies with applied resonant fields on TEXT. Nucl Fusion 1989;29:547.
[7] Meiss JD. Symplectic maps, variational principles, and transport. Rev Mod Phys 1992;64:795–848.
[8] Karger F, Lackner F. Resonant helical divertor. Phys Lett A 1977;61:385–7.
[9] Engelhardt W, Feneberg W. Influence of an ergodic magnetic limiter on the impurity content in a tokamak. J Nucl Mater 1978;76/77:518.
[10] Feneberg W, Wolf GH. A helical magnetic limiter for boundary-layer control in large tokamaks. Nucl Fusion 1981;27:669–76.
[11] Whiteman KJ. Invariants and stability in classical mechanics. Rep Prog Phys 1977;40:1033–69.
[12] Hazeltine RD, Meiss JD. Plasma confinement. Reading, MA: Addison-Wesley; 1992.
[13] Viana RL. Chaotic magnetic field lines in a tokamak with resonant helical windings. Chaos, Solitons & Fractals 2000;11:765–78.
[14] Lichtenberg AJ, Lieberman MA. Regular and chaotic dynamics. 2nd ed. NewYork, Berlin, Heidelberg: Springer; 1992.
[15] Martin TJ, Taylor JB. Ergodic behaviour in a magnetic limiter. Plasma Phys Controlled Fusion 1984;26:321.
[16] Ohyabu N, deGrassie JS, Brooks NH, et al. J Nucl Mater 1984;121:363.
[17] Punjabi A, Verma A, Boozer A. Stochastic broadening of the separatrix of a tokamak divertor. Phys Rev Lett 1992;69:3322.
[18] Ghendrih Ph, Grosman A, Capes H. Theoretical and experimental investigations of stochastic boundaries in tokamaks. Plasma Phys Controlled Fusion 1996;38:1653–724.
[19] Punjabi A, Ali H, Boozer A. Symmetric simple map for a single-null divertor tokamak. Phys Plasmas 1997;4:337.
[20] Abdullaev SS, Finken KH, Kaleck A, Spatschek KH. Twist mapping for the dynamics of magnetic field lines in a tokamak ergodic divertor. Phys Plasmas 1998;5:196.
[21] Abdullaev SS, Finken KH, Spatschek KH. Asymptotical and mapping methods in study of ergodic divertor magnetic field in a toroidal system. Phys Plasmas 1999;6:153.
[22] Balescu R, Vlad M, Spineanu F. Tokamap: a Hamiltonian twist map for magnetic field lines in a toroidal geometry. Phys Rev E 1998;58:951.
[23] Balescu R. Hamiltonian nontwist map for magnetic field lines with locally reversed shear in toroidal geometry. Phys Rev E 1998;58:3781.
[24] Viana RL, Caldas IL. Peripheral stochasticity in tokamaks – the Martin–Taylor model revisited. Z Naturforsch 1992;47a:941–4.
[25] Ullmann K, Caldas IL. A symplectic mapping for the ergodic magnetic limiter and its dynamical analysis. Chaos, Solitons & Fractals 2000;11:2129–40.
[26] Caldas IL, Pereira JM, Ullmann K, Viana RL. Magnetic field line mappings for a tokamak with ergodic limiters. Chaos, Solitons & Fractals 1996;7:991–1010.
[27] Viana RL, Vasconcelos DB. Field-line stochasticity in a tokamak with an ergodic magnetic limiter. Dyn Stability Syst 1997;12:75–88.
[28] da Silva EC, Caldas IL, Viana RL. The structure of chaotic magnetic field lines in a tokamak with external nonsymmetric magnetic perturbations. IEEE Trans Plasma Sci 2001;29:617–31.
[29] da Silva EC, Caldas IL, Viana RL. Field line diffusion and loss in a tokamak with an ergodic magnetic limiter. Phys Plasmas 2001;8:2855–65.

[30] Kucinski MY, Caldas IL. Toroidal helical fields. Z Naturforsch 1987;42a:1124–32.
[31] Morse PM, Feshbach H. Methods of theoretical physics, vol. 2. New York: McGraw-Hill; 1953.
[32] Kucinski MY, Caldas IL, Monteiro LHA, Okano V. Toroidal plasma equilibrium with arbitrary current distribution. J Plasma Phys 1990;44:303–11.
[33] Escande DF. Stochasticity in classical Hamiltonian systems: universal aspects. Phys Rep 1985;121(3–4):165–261.
[34] Greene JM. A method for determining a stochastic transition. J Math Phys 1979;20:1183–201.
[35] Chirikov BV. A universal instability of many-dimensional oscillator systems. Phys Rep 1979;52:265–379.
[36] Mackay RS, Meiss JD, editors. Hamiltonian dynamical systems. Bristol: Adam Hilger.
[37] Ruelle D, Eckmann JP. Ergodic theory of chaos and strange attractors. Rev Mod Phys 1985;57:617–56.
[38] Greene JM. Renormalization and the breakup of magnetic surfaces. In: Horton Jr CPW, Reichl LE, editors. Statistical physics and chaos in fusion plasmas. New York: Wiley; 1984.
[39] Finn JM. $q = 2$ Resonant bifurcations for tokamak field lines, period doubling and field line chaos. Comments Plasma Phys Controlled Fusion 1991;14(3):149–64.
[40] Mackay RS. A renormalization approach to invariant circles in area-preserving maps. Physica D 1983;7:283.
[41] Abdullaev SS. A new integration method of Hamiltonian systems by symplectic maps. J Phys A: Math Gen 1999;32:2745–66.